ORIGINAL PAPER

Investigation of triplex CaAl$_2$ZnO$_5$ nanocrystals on electrical permittivity, optical and structural characteristics of PVA nanocomposite films

H. M. Gayitri[2] · Murad AL-Gunaid[3,4] · Siddaramaiah[4] · A. P. Gnana Prakash[1]

Abstract

Nanocomposite (NC) films of polyvinyl alcohol (PVA)/calcium aluminum-doped zincate (CaAl$_2$ZnO$_5$) have been fabricated with varying amounts, namely 2, 4, 6 and 8 wt% of CaAl$_2$ZnO$_5$ nanoparticles (NPs) by solution casting technique. TEM data showed that an average particle size of CaAl$_2$ZnO$_5$ NPs is ~ 25 nm. The effect of CaAl$_2$ZnO$_5$ content on structural and morphological behaviors has been established by Fourier-transform infrared spectroscopy and scanning electron microscopy, respectively. The photo-response of NCs was derived by UV–visible spectroscopy where the band gap energy (E_g) reduced from 5.25 eV for PVA to 2.82 eV for PVA/8 wt% CaAl$_2$ZnO$_5$ NC film. The dielectric permittivity and current–voltage (I–V) characteristics were studied using LCR—meter in frequency range of 50 Hz–5000 kHz. The relative dielectric constant (ε') was increased from 15 to 65 with increase in NPs content from 0 to 8 wt%. The PVA NC with 8 wt% CaAl$_2$ZnO$_5$NPs raises the ac conductivity to 3.35×10^{-5} S cm^{-1} at room temperature. The cyclic voltammetry (CV) tests have been performed to calculate the specific capacitance of the NCs as a positive electrode against Ag/AgCl as reference electrode. The specific capacitance increases from 1. Fg^{-1} for PVA to 3.69 Fg^{-1} for PVA/8 wt% CaAl$_2$ZnO$_5$ NC. These behaviors will support the possible applications in optical display devices and micro-electrical and electronic applications.

Keywords CaAl$_2$ZnO$_5$NPs · Band gap · Dispersion energy · Dielectric permittivity · Specific capacitance

✉ A. P. Gnana Prakash
    gnanaprakash@physics.uni-mysore.ac.in

Extended author information available on the last page of the article

Introduction

In the recent years, semiconductor nanoparticles (NPs) have attracted much attention worldwide due to their outstanding opto-electrical and mechanical properties. Among various inorganic semiconductor compounds, zinc oxide (ZnO) has stable wurtzite structure with wide direct band gap and high binding energy. Due to its excellent properties, it has a broad range of potential applications, e.g., in ultraviolet (UV) light emitters, transparent electronics, piezoelectric devices, chemical sensors and spin electronics [1–3]. Many studies have focused on the synthesis and development of ZnO as transparent conducting oxides (TCOs) using a range of techniques and dopants, such as Li, Al, Ni and Ga [4–7] to improve the electrical conductivity without degrading their optical transmission. Calcium zincate is a semiconductor with wide band gap energy, transparent in the visible regions and is excellent UVA shielding materials owing to their direct band gap absorptions. Furthermore, alkali and alkaline earth metal-doped ZnO are known to emit visible luminescence arising from intrinsic structural characteristics besides exciton emission [8]. The *p*-type based on aluminum-doped ZnO (AZO) materials has significantly attracted because it is non-toxic and inexpensive. The NPs consisting of zinc oxide and aluminum exhibit high transparency enhanced electrical, thermal and chemical stability [9, 10]. More recently, mixed metal oxides, composed of three or more metal elements with similar radii, are expected to have a stronger synergetic effect in comparison with the corresponding binary metal oxides [11, 12]. Transition metal oxide NPs-loaded polymer-based nanocomposite materials are promising candidates which have been constantly developed and investigated to meet newer challenges for opto-electrical applications. One of the most important challenges in the development of nanocomposites is concerned on reducing optical bandwidth, arising refractive index and improving electrical properties which are desirable for opto-electronic application. The filling up of weak micro-regions of the polymer matrix by NPs may enhance the interaction at the polymer–filler interfaces [13, 14]. Among the above-mentioned NPs, calcium aluminum zincate NPs have preferred to use strong oxidizing agent of photo-generated holes, chemical inertness, non-toxicity, low cost, high refractive index (RI) and good dispersing ability in polymeric system [15].

The optical properties on the NCs are different from their individual components. If these hybrid NPs are well dispersed in a matrix, the intrinsic properties of a nanostructured material are determined by its size, shape, composition, crystallinity and structure property relationships of polymer can also be tuned for tailor-made applications. Polyvinyl alcohol (PVA) is a semicrystalline polymer with highly transparent, flexible, good mechanical properties and easy film forming; in addition, its polar hydroxyl group is known to offer excellent filler dispersions owing to its excellent particle stabilizing nature. Furthermore, PVA is also known to undergo photochemical transformations under the influence of high energy radiations [16]. This distinctive feature of PVA can also affect the properties of NCs, since material characteristics of semiconductor, especially optical absorption, emission and electronic conduction, are known to be influenced

significantly by the extent of passivation of under coordinated surface atoms of the semiconductor by organic ligands in addition to the chemical nature of entities [17]. Bouropoulos et al. [18] reported that 2.5 wt%ZnO NPs embedded in PVA caused to enhance absorption of incident light and reducing NCs band gap energy into 3.2 eV. Subramani et al. [19] have investigated on calcium zincate PVA/Ca$_{0.2}$Zn$_{0.8}$O NC films which exhibited appreciable UVA screening efficacies with maximum absorption in the UVA regions. The band gap energy reduced to less than 3.1 eV and refractive index enhanced to 3 at 400 nm, whereas ac conductivity increased to 7.5×10^{-4} S cm^{-1} at higher frequency for PVA/4 wt% Ca$_{0.2}$Zn$_{0.8}$O. In our previous work, ternary metal oxide CaNiAl$_2$O$_5$ NPs-doped PVA matrix was fabricated where the band gap energy is reduced from 5.1 eV for pure PVA to 2.8 eV for 8 wt% NPs-loaded PVA NCs with improved optical and electrical behaviors [20]. The motivation of our work is to further improve the desired properties of polymer nanocomposites (NCs) by incorporation of hybridized metal oxide NPs includes alkali, alkali earth metals and transitional metals. The incorporation of such NPs into polymer matrix to form nanocomposites (NCs) is a unique way of improving polymer properties for tailor-made applications. In the current research work, CaAl$_2$ZnO$_5$ has been synthesized by solution combustion method as new tertiary NPs to investigate its effect on structural, microcrystalline, optical parameters, electrical and electrochemical behaviors of PVA NCs.

Experimental

Materials

PVA (average molecular weight 125,000 Aldrich), calcium(II) nitrate tetrahydrate Ca(NO$_3$)$_2$·4H$_2$O), nickel(II) nitrate hexahydrate (Ni (NO$_3$)$_3$·6H$_2$O), aluminum(III) nitrate trihydrate (Al(NO$_3$)$_2$·3H$_2$O) (as oxidants) and glycine (C$_2$H$_5$NO$_2$) (as fuel) were purchased from SD fine-chemicals Limited, Mumbai, India. Double-distilled water was used in this study.

Synthesis of (Ca$_{0.2}$Al$_{0.3}$Zn$_{0.5}$O$_x$) nanoparticles

The nanopowder was synthesized using sol–gel technique via combustion method [21]. The appropriate quantity 1.18 g of calcium nitrate Ca(NO$_3$)$_2$, 1.87 g of aluminum nitrate Al(NO$_3$)$_3$ and 2.87 g of zinc nitrate Zn(NO$_3$)$_2$ were dissolved separately in double-distilled water under constant stirring (900 rpm) on magnetic stirrer for 30 min. The fuel (molar ratio of fuel/metal nitrates as oxidant is 2:1) was dissolved separately in double-distilled water with constant stirring on magnetic stirrer. The individual solution then mixed together with continuous stirring by magnetic stirrer for 2 h at 60 °C and then added fuel to the mixture. The pH of the media was maintained at 7 by adding drop wise 10 ml of 0.1 M NaOH. Then, the reaction mixture was kept for vigorous stirring at 90 °C for 2 h until dark gel was obtained. The

gel further heated until combustion process occurs to obtain a fine powder. Finally, the light cream color powder has been calcinated at 650–800 °C for 2 h to remove undesirable reagents and the nanopowder becomes more stable.

Preparation of PVA/CaAl$_2$ZnO$_5$ nanocomposite films

The varying amounts, namely 2, 4, 6 and 8 wt% of NPs, were added to aqueous 7 wt% PVA solution by stirring followed by ultrasonication for 30 min. The solution thus obtained was poured into a cleaned glass mold and dried gradually at room temperature. The obtained NC films were transparent and free from air bubbles. Finally, the samples were vacuum-dried in a hot air oven at 60 °C for 3–4 h. The thickness of the films obtained lies in the range 0.19–0.23 mm.

Techniques

The surface morphological behaviors of NCs were recorded after gold coat by scanning electron microscope (SEM), Zeiss-108A, Germany. The physical interaction between components was studied by Fourier-transform infrared (FTIR) spectroscopy, recorded at a resolution of 2 cm^{-1} and 32 scans in the wave number range 4000–500 cm^{-1} employing JASCO 4100 spectrometer, Japan. The morphological behavior of CaAl$_2$ZnO$_5$ NPs has been evaluated by transmission electron microscope (TEM) with JEOL/JEM 2100, Japan. The microstructure of pure CaAl$_2$ZnO$_5$ NPs and its NCs with PVA were obtained by X-ray diffraction (XRD) by Advance Brucker AXS diffractometer equipped with CuKα radiation source ($\lambda = 1.5406$ Å) in the 2θ range 5°–60° in step of 0.02. The optical properties were characterized by UV–visible spectrophotometer, in the wave number range 230–800 nm, Shimadzu-1800, Japan. Electrochemical cyclic voltammetry (CV) and galvanostatic charge–discharge were performed using CH Instrument, model 600D series, with potassium hydroxide (2 M) as background electrolyte at potential scan rate of 0.1 V s^{-1} using Ag/AgCl reference and platinum wire as counter electrodes. The electrical (I–V and AC) parameters of films were measured with applied voltage of 1 V and operating frequency range 50 Hz–5000 kHz at room temperature by LCR–meter, Wayne Kerr-6430, UK. The surface of films was coated with silver paste and sandwiched between two stainless steel electrodes which have an area of 0.5 cm^2. The values of capacitance (C), resistance (R), conductance (Gs) and dissipation factor (tan δ) of the NC films at each excitation frequency were recorded at room temperature.
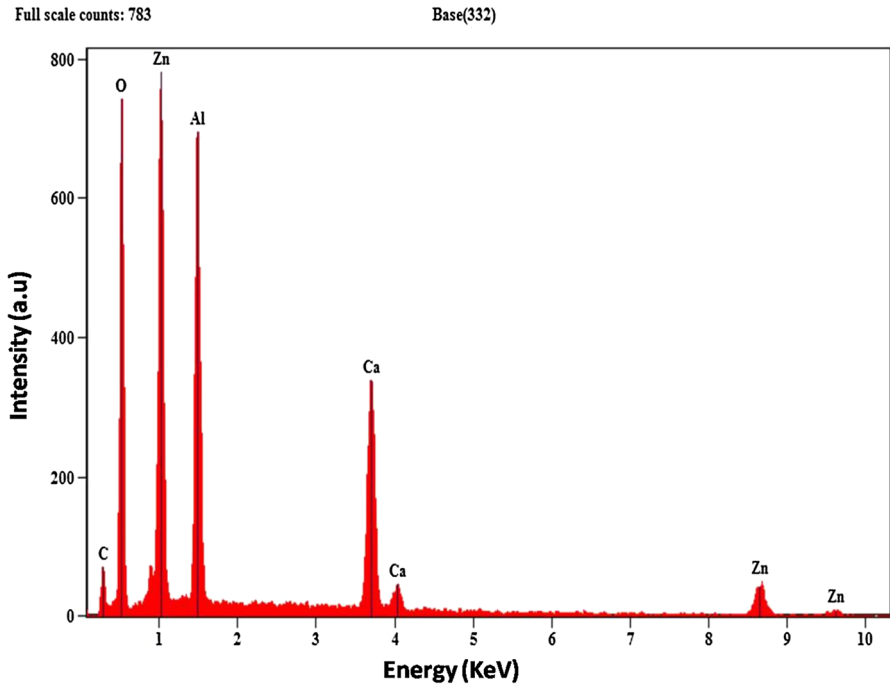
Fig. 1 The EDX spectra of CaAl$_2$ZnO$_5$ NPs

Table 1 Elemental composition obtained from EDS

Elements	wt%	wt% error (±)	Atom (%)
C K	13.89	0.72	23.39
O K	43.42	0.74	54.90
Al K	14.24	0.23	10.67
Ca K	11.45	0.29	5.78
Ca L	–	–	–
Zn K	16.99	1.54	5.26
Zn L	–	–	–
Total	100.00		100

Results and discussion

Morphological and structural analysis

EDS

The energy-dispersive spectrum (EDS) of prepared CaAl$_2$ZnO$_5$ NPs is illustrated in Fig. 1, which reveals the atomic % and weight % of the individual elemental
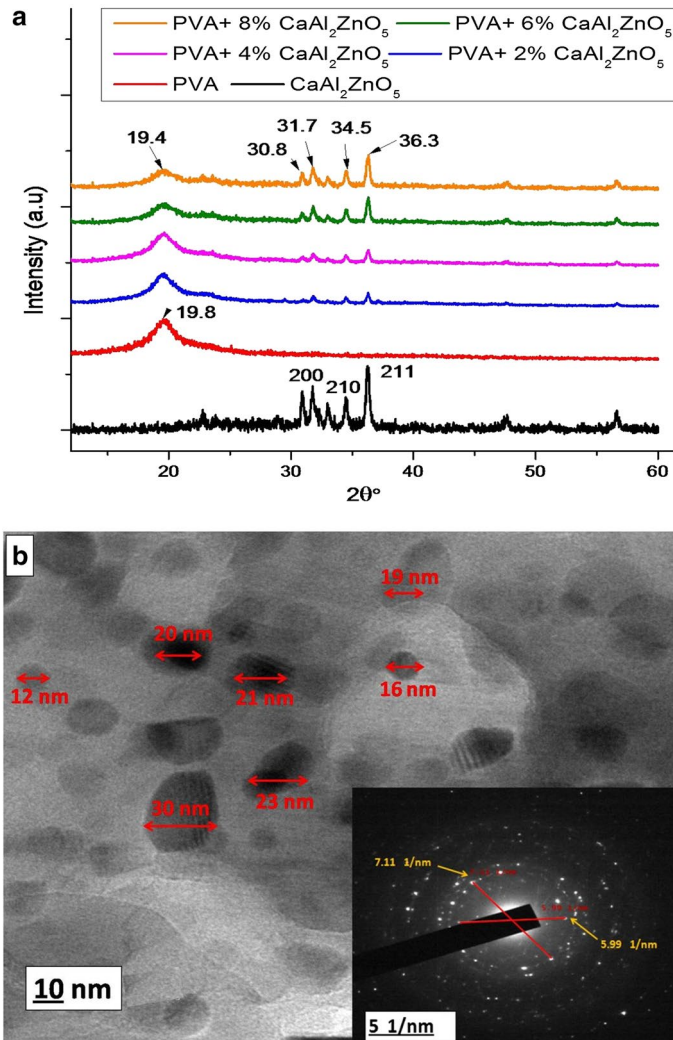
Fig. 2 **a** XRD patterns for PVA/CaAl$_2$ZnO$_5$ nanocomposites and **b** TEM image of CaAl$_2$ZnO$_5$ NPs

composition. The obtained weight and atomic percentage of NPs from EDS spectrum are listed in Table 1. The obtained results indicate the existence of triple metals in the metal oxides where the percentage of Al and Zn are major and Ca is the minor component in NPs.

XRD and TEM

The XRD profiles of pristine CaAl$_2$ZnO$_5$ NPs and PVA NCs with 0, 2, 4, 6 and 8 wt% of NPs are displayed in Fig. 2a. The diffraction peak at $2\theta = 19.8°$ ($hkl = 101$) is referred to crystalline nature in PVA due to H bond in its structure. The sharp major crystalline

peaks for $CaAl_2ZnO_5$ NPs are observed at $2\theta=31.6°$, $34.6°$ and $36.6°$ with corresponding hkl values of 200, 201 and 211. The intensity of the relative diffraction peaks of the NCs was an indicator of the structural changes of the polymer matrix. The intensity of the diffraction peak becomes smaller and broader as increase in the NPs in PVA matrix. This indicates that the NCs have disorder structure which enhances its ionic conductivity [22]. From Fig. 2a, at $2\theta=20°$ a small shift in the peak position with significant reduction in intensity for the NCs was observed. This can be attributed to the physical interaction between NPs and PVA matrix. The Scherrer lengths (L) of the pristine NPs have been calculated using Scherrer formula (1);

$$L = \frac{K\lambda}{Cos\theta} \tag{1}$$

where K is the constant ($K=0.9$), which is related to the crystallite shape; λ and θ are the radiation wavelength and Bragg's angle, respectively; and β is the full width at half maximum of the diffraction peak. The average particle size calculated using Scherrer formula is 22 nm for $CaAl_2ZnO_5$ NPs [23], which has good agreement with the TEM result as displayed in Fig. 2b. TEM image (Fig. 2b) reveals that the average particle size of $CaAl_2ZnO_5$ NPs is 25 nm with a small dispersive spherical and porous shape. The porosity was observed on the surface of NPs, which may be due to release of gases during the synthesis of NPs by combustion process.

The percentage porosity ($\%\varepsilon$) of pure NPs has been determined using procedure reported elsewhere [24]. The sample was soaked in n-butanol, and the porosity was estimated using the sample weight before and after drying according to Eq. (2) as follows:

$$\%\varepsilon = \frac{(w_B - w_A)/\rho_B}{w_A/\rho_A + (w_B - w_A)/\rho_B} \tag{2}$$

where W_B is the weight of the sample before drying, W_A is the weight of the sample after drying (g), ρ_B is the density of n-butanol (0.81 g/cm^3), and ρ_A is the density of pure $CaAl_2ZnO_5$ NPs which is 1.33 g/cm^3. The obtained result of calculated $\%\varepsilon$ for pristine NPs is 90.4%.

The morphological behaviors of PVA/$CaAl_2ZnO_5$ NC films have been studied by SEM images, where it ascertains the morphological compatibility between the host polymer and the metal oxide NPs [25]. The SEM image of $CaAl_2ZnO_5$ NPs clearly indicates the agglomerated and circular/spherical shape as shown in Fig. 3a. The SEM images of pure PVA and its NCs with 2, 4, 6 and 8 wt% of $CaAl_2ZnO_5$ NPs are displayed in Fig. 3b–f, respectively. It can be noticed that NPs are homogeneously dispersed throughout the PVA matrix at lower dosages but slightly agglomerated form at higher dosage of NPs due to increase in filler–filler interaction.

FTIR

The FTIR spectroscopy is used to determine the interaction between the components present in the NC films. The FTIR spectra of pure PVA and PVA/$CaAl_2ZnO_5$

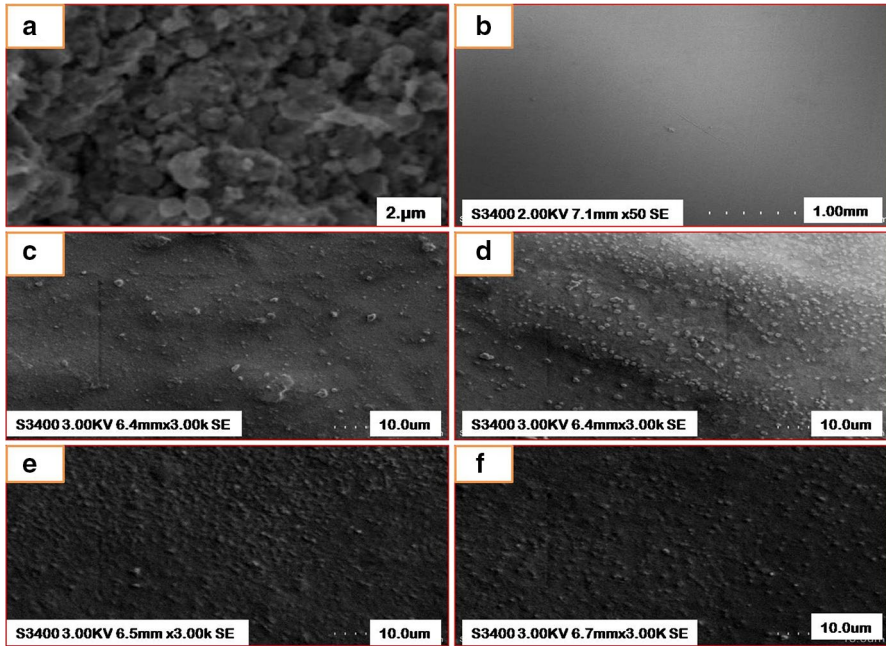**Fig. 3** SEM photomicrographs of **a** $CaAl_2ZnO_5$ NPs, **b** pure PVA, PVA with **c** 2, **d** 4, **e** 6 and **f** 8 wt% of $CaAl_2ZnO_5$ nanocomposites
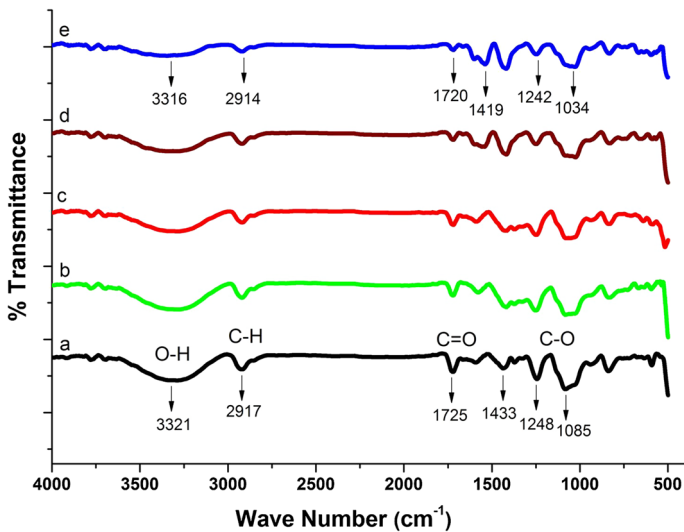

Fig. 4 FTIR spectra of PVA nanocomposite films with (a) 0, (b) 2, (c) 4, (d) 6 and (e) 8 wt% of $CaAl_2ZnO_5$ NPs

Table 2 Asymmetrical shifts observed in FTIR spectra of pure PVA and its NCs

wt% of CaAl$_2$ZnO$_5$ in PVA	O–H (str. vib.)* cm^{-1}	(C–H) (str. vib.) cm^{-1}	C=O (str. vib.) cm^{-1}	C–O (str. vib.) cm^{-1}
0	3321	2917	1725	1085
2	3319	2916	1732	1073
4	3318	2915	1722	1064
6	3315	2914	1721	1040
8	3316	2914	1720	1034

*(str. vib.) is stretching vibration

NCs are displayed in Fig. 4a–e. From Fig. 4a, an intense broadband observed at 3321 cm^{-1} corresponds to O–H stretching vibration associated with PVA molecule [26]. The decrease in the intensities of O–H stretching vibration and the broadening of the peak in NCs may be referred to the electrostatic interactions between the surface charges on the metallic fractals of the NPs and O–H groups of PVA [27]. The absorption peak at around 2914 cm^{-1} and 1725 cm^{-1} may be due to CH bond and C=O stretching vibration, respectively. The absorption band around 1085 cm^{-1} may be due to single C–C bond stretching mode of acetyl group. It was observed that FTIR spectra of NCs exhibit several irregular shifts in peak position with varying intensities of pure PVA as presented in Table 2. The shifts in peak position indicated in the spectra are mainly because of the orderly arranged hydroxyl groups of the PVA chain accomplished by forming stable complex compounds with NPs [28]. The observed variation may also be related to defects generated by the charge-transfer
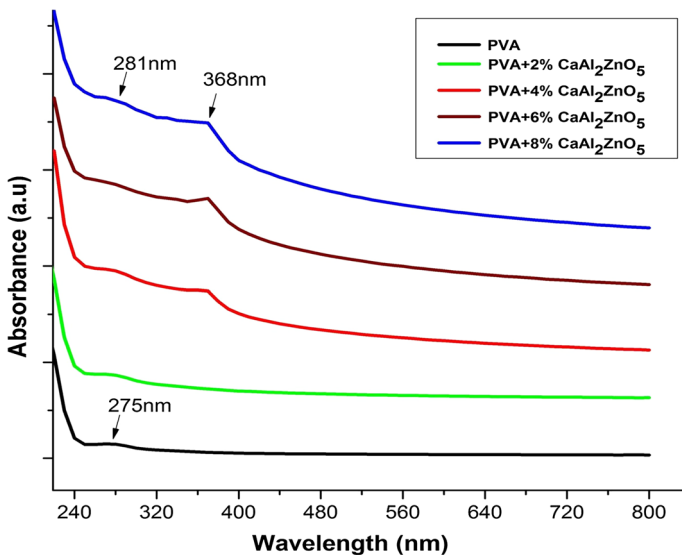

Fig. 5 Absorbance spectra of PVA/CaAl$_2$ZnO$_5$ nanocomposites as a function of wavelength

complex (CTC) existing between NPs and PVA chain [29]. These justifications strengthen the interactions between $CaAl_2ZnO_5$ NPs and functional groups of PVA matrix.

UV–Vis analysis

The UV–Visible absorption spectroscopy is a technique to examine the optical properties of nano-sized particles and its NCs. Figure 5 depicts the UV–Visible absorption spectra of pure PVA and its NC films in the wavelength range 200–800 nm. Figure 5 reveals that the pure PVA exhibits one broad absorbance band at 275 nm and one weak band or shoulder at 281 nm and these bands are assigned to the electronic transitions, $\pi \rightarrow \pi^*$ and $n \rightarrow \pi^*$, respectively [30]. The
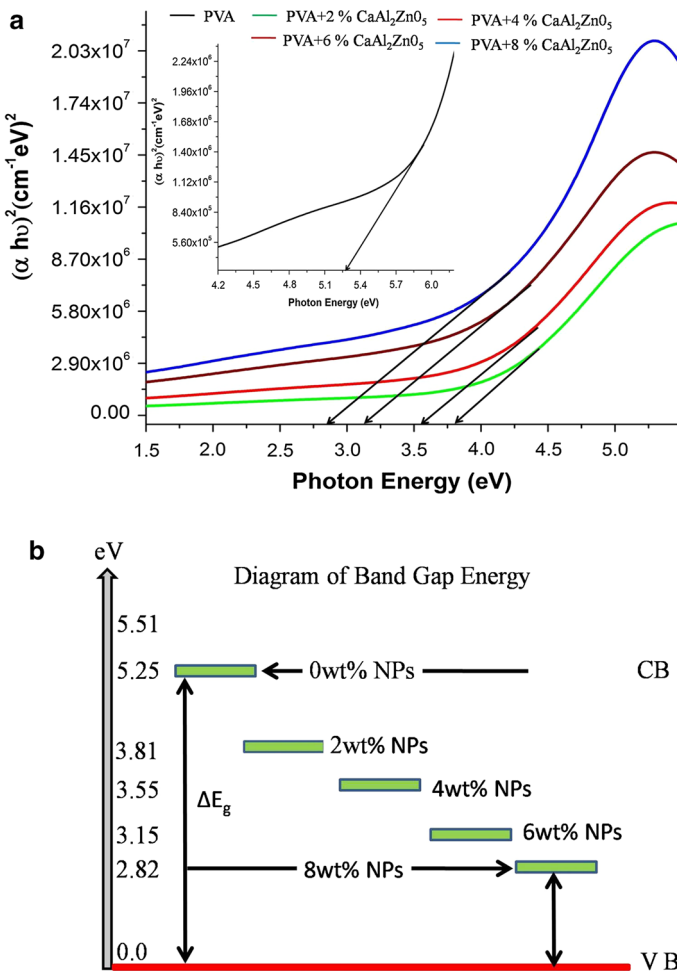

Fig. 6 **a** Tauc's plot and **b** band gap energy diagrams of PVA/$CaAl_2ZnO_5$ nanocomposites

Table 3 Optical parameters of CaAl$_2$ZnO$_5$ NCs

wt% of CaAl$_2$ZnO$_5$ in PVA	n at $\lambda_{360\ nm}$ ± 0.04	E_g (eV) ± 0.12	E_0 (eV) ± 0.45	E_d (eV) ± 0.56
0	1.31	5.25	7.87	12.34
2	1.36	3.81	5.71	16.63
4	1.64	3.55	5.32	21.32
6	2.12	3.15	4.72	25.89
8	2.43	2.82	4.23	27.24

absorption spectra of the PVA and PVA/CaAl$_2$ZnO$_5$ NC films exhibit the signature peaks of PVA at 275 and 281 nm, and further, the absorbance band at 368 nm corresponds to CaAl$_2$ZnO$_5$ NPs, which will be blue shift (7 nm) compared with ZnO bulk material (380 nm) at room temperature. This blue shift is due to the quantum confinement effect, which can be attributed to the reduction in the crystallite size [31]. It validates the presence of CaAl$_2$ZnO$_5$ NPs. The increasing light absorbance of the NC films with increase in NPs content is because of the added NPs that absorbs the incident radiation [32].

The plots of $(\alpha hv)^2$ as a function of photon energy are displayed in Fig. 6a. The obtained values of E_g are tabulated in Table 3. The incorporation of higher dosage of NPs into PVA matrix creates defects in band gap level. This can be attributed to the morphological changes in the PVA structure. The optical band gap energy can be obtained from the optical absorption spectrum using the following Eq. (3);

$$\alpha hv = C\left(hv - E_g\right)^r \tag{3}$$

where C is a constant, E_g is the optical band gap energy of the material and the exponent, r, is an index that depends on the nature of electronic transition, where $r = 1/2$ for direct allowed transitions, $r = 3/2$ for direct forbidden transitions, $r = 2$ for indirect allowed transitions, and $r = 3$ for indirect forbidden transitions. For pure PVA, the energy band gap is high between valance and conduction band, so direct forbidden transition. However, the absorption edge of transition is blue shift, meaning that the band gap was reduced with increase in NPs up to 8 wt% in PVA matrix with sharp higher absorption at 3.5 eV, hence the direct allowed transitions. The decrease in E_g with increase in CaAl$_2$ZnO$_5$ content is displayed in Fig. 6b. Such decrease in band gap can be due to strong physical interaction between CaAl$_2$ZnO$_5$ and PVA, which form the bridge between the highest occupied molecular orbital (HOMO) and the lowest unoccupied molecular orbital (LUMO) energy states, making the lower energy transitions suitable and results in the reduction in the optical band gap energy [33, 34]. The minimum E_g value achieved in the current investigation is 2.82 eV for PVA/8 wt% CaAl$_2$ZnO$_5$, which is significantly smaller than that reported for PVP/8 wt% CsAlO$_2$ NCs ($E_g = 4.86$ eV) elsewhere [35].

The refractive index (n) plays a major role in optical communication and design of the optical instruments [36]. The variation of n as a function of photon energy of PVA/CaAl$_2$ZnO$_5$ NCs is displayed in Fig. 7a. The n can be determined using Eq. (4)
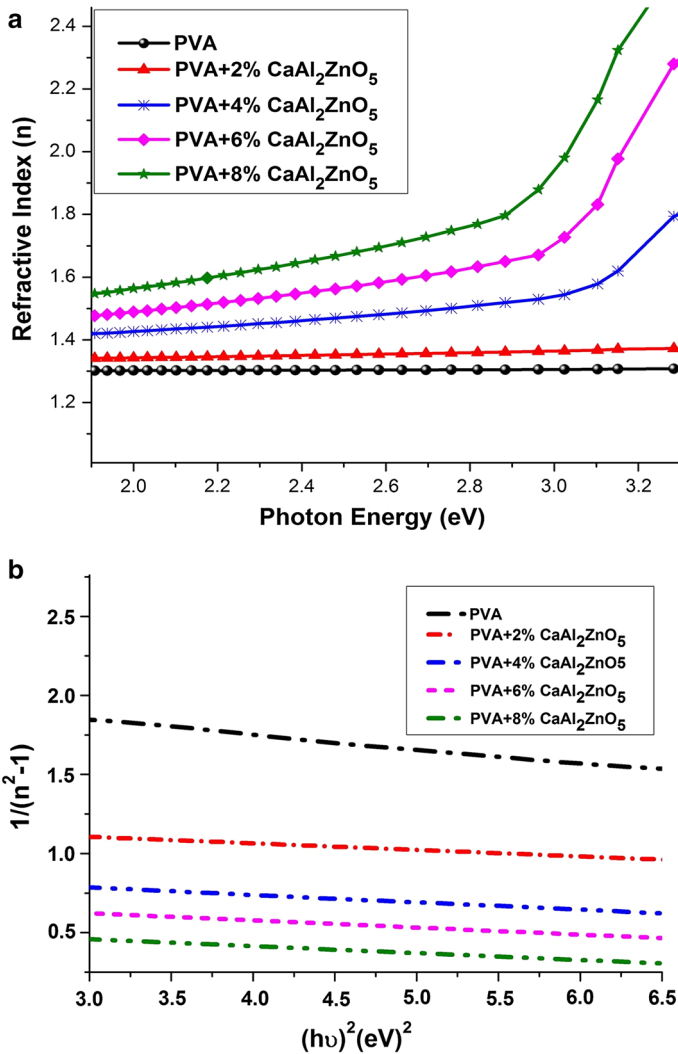
Fig. 7 Plots of **a** refractive index for PVA/CaAl$_2$ZnO$_5$ nanocomposites as a function of photon energy and **b** $(n^2 - 1)^{-1}$ as a function of $(h\upsilon)^2$

$$n = \frac{(1 + R) + \sqrt{4R - (1 - R^2)K^2}}{1 - R} \qquad (4)$$

where R is reflectance and K is extinction coefficient.

The n values increase with increase in NPs content due to increase in packing density of the NC films as shown in Fig. 7a. Incorporation of NPs in PVA matrix will increase the polarization of dipoles in NCs, leading to increased refractive index (n).

The NCs with higher n values are very useful in optics and photonics due to their ability to reduce reflection losses at interfaces, which leads to increase in optical output. The refractive index for PVA/8 wt% $CaAl_2ZnO_5$ is higher by 1.12 magnitudes than that of pure PVA matrix [37]. The applications of materials with higher n values include anti-refractive coatings, micro-lenses for complementary metal oxide semiconductor, image sensors and encapsulate for LEDs [38].

The n dispersion has been analyzed using the oscillator model developed by Wemple and DiDomenico (WD). It was determined using Eq. (5) [39],

$$n^2 - 1 = \frac{E_0 E_d}{E_0^2 - (hv)^2} \tag{5}$$

where E_0 is the oscillator energy, which is a measure of average excitation energy for electronic transitions, and E_d is the dispersion energy, which is a measure of the average strength of inter-band optical transitions. The values of E_0 and E_d can be obtained from the intercept (E_0/E_d) and slope ($-1/E_0 E_d$) of the linear fitted lines from the plots of $1/(n^2-1)$ versus $(hv)^2$ as shown in Fig. 7b. The estimated values of E_0 and E_d for all films are addressed in Table 3. The values of oscillator energy, E_0, decrease with increase in NPs concentration in PVA matrix, where the E_0 is empirically related to the lowest optical band gap as; $E_0 \sim 1.5E_g$ [40]. The dispersion energy, E_d, is associated with changes in the structural order of the material [41]. The increase in E_d values of NCs with increase in $CaAl_2ZnO_5$ content was noticed.

Cyclic voltammograms studies

Cyclic voltammograms (CV) were recorded at room temperature by employing three-electrode cell with platinum wire as an auxiliary electrode, Ag/AgCl electrode as the reference electrode and NC films as the working electrode. The CVs were obtained in 2 M KOH electrolyte solution. The scanning was carried out in the voltages range from 0 to 1 V at scan rate of 10 mV s^{-1}. The effect of varying scan rate from 10 to 100 mV s^{-1} has been studied in 2 M KOH for pristine PVA and PVA/8 wt% $CaAl_2ZnO_5$ as displayed in Fig. 8a. The performance of an electrochemical capacitor in terms of electrochemical behavior and the charge storage at individual interfaces in anodic and cathodic regions can be examined by CV [42, 43]. With increase in scan rate, the peak current separation increased and also the peak potential shifted slightly, the anodic peak toward positive and the cathodic peak toward negative potential directions. Figure 8b indicates the CV curves of pristine PVA and PVA/8 wt% $CaAl_2ZnO_5$ at fixed scan rate of 10 mV s^{-1} with a potential range 0–1 V. The CV profiles of two-electrochemical-capacitor (ECs) cell are nearly rectangular in shape. There is no higher distinct region along the oxidation and reduction path. It denotes that the electron-transfer process or redox reactions are absent in both cells, but the excellent CV curves reveal a rapid current response on voltage reversal at each end potential. The straight rectangular sides represent a very small equivalent series resistance (ESR) of the electrodes with fast diffusion of electrolyte in the films.
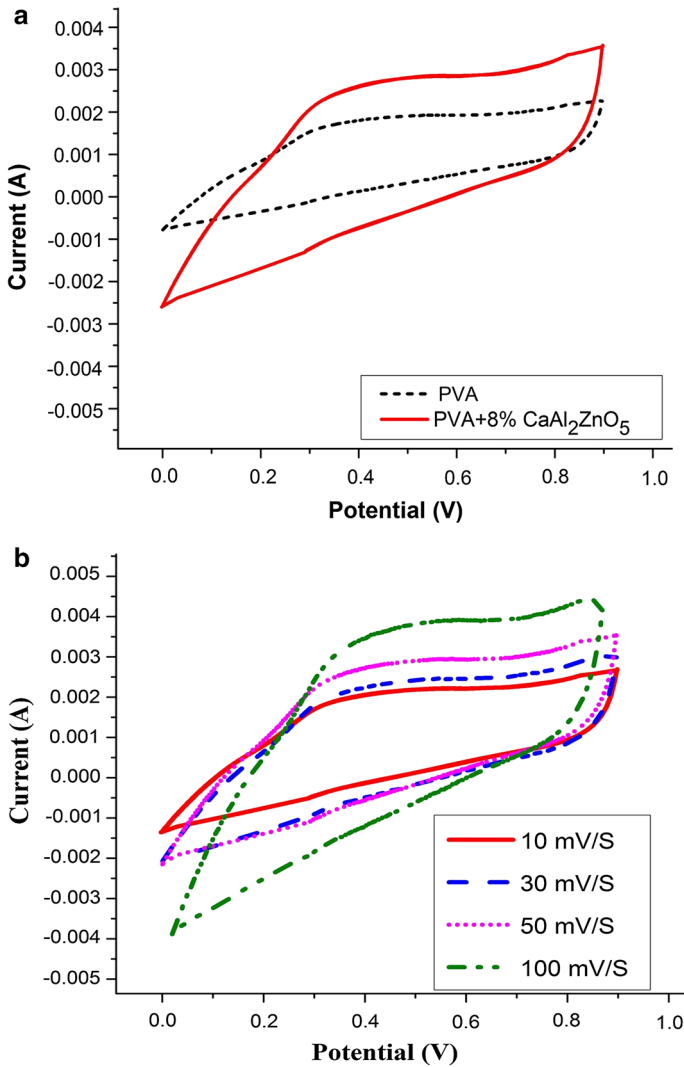
Fig. 8 CV curve of **a** pure PVA and PVA/8 wt% CaAl$_2$ZnO$_5$ NCs at 10 mV/S **b** PVA/8 wt% CaAl$_2$ZnO$_5$ NCs at different scan rates

The specific capacitance, C_{spec}, can be calculated from the CV profile using Eq. (6)

$$C_{spec} = \frac{i}{Vm} \qquad (6)$$

where i is the average current (A), V is the scan rate (V s^{-1}), and m is the mass of the electrode material. The C_{spec} of EC cell with PVA and EC cell with PVA/8 wt% CaAl$_2$ZnO$_5$ electrode are 1.68 and 2.9 F g^{-1}, respectively. The EC cell with
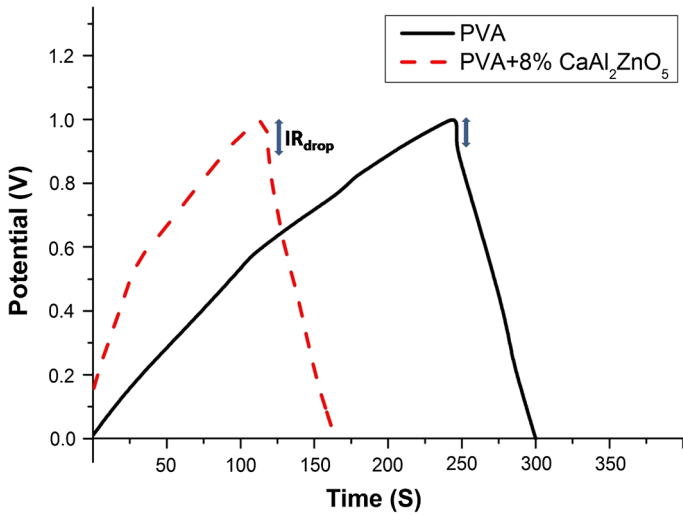
Fig. 9 Charge–discharge curve of pure PVA and PVA/8 wt% CaAl$_2$ZnO$_5$ nanocomposites

PVA/8 wt% CaAl$_2$ZnO$_4$ exhibits higher specific capacitance as compared to EC cell with pure PVA. This indicates that the addition of NPs into polymer matrix will enhance the capacitance values.

Figure 9 shows the charge–discharge curves of pristine PVA and PVA/8 wt% CaAl$_2$ZnO$_5$NC at the current density of 10 mA cm^{-2}. The charge–discharge curves exhibit mirror-like images, indicating a reversible oxidation process and better electrochemical capacitance performance. This explains that charge and discharge occur reversibly for NC at the electrode–electrolyte interface.

Electrical studies

Ac conductivity, σ_{ac}, values of NC films as a function of the CaAl$_2$ZnO$_5$ NPs content and frequency are plotted in Fig. 10a, b, respectively. It was observed in Fig. 10a, b that σ_{ac} of PVA host matrix increases with increase in filler loading and frequency. This clearly shows that the addition of CaAl$_2$ZnO$_5$ NPs enhances the polar characteristics of PVA matrix. The rise in ac conductivity with frequency is a common phenomenon for polymeric and semiconductive samples [44]. The homogeneous dispersion of nanofiller in PVA matrix generates a conductive path inside PVA film and leads to diffusion of electrons from one site to another site; hence, conductivity increases in NC films. Further, as frequency increases, the electrons get sufficient energy to transfer through energy gap to conduction band of NC films caused to raise conductivity.

The ac conductivity of the sample is estimated from Eq. (7) [45].
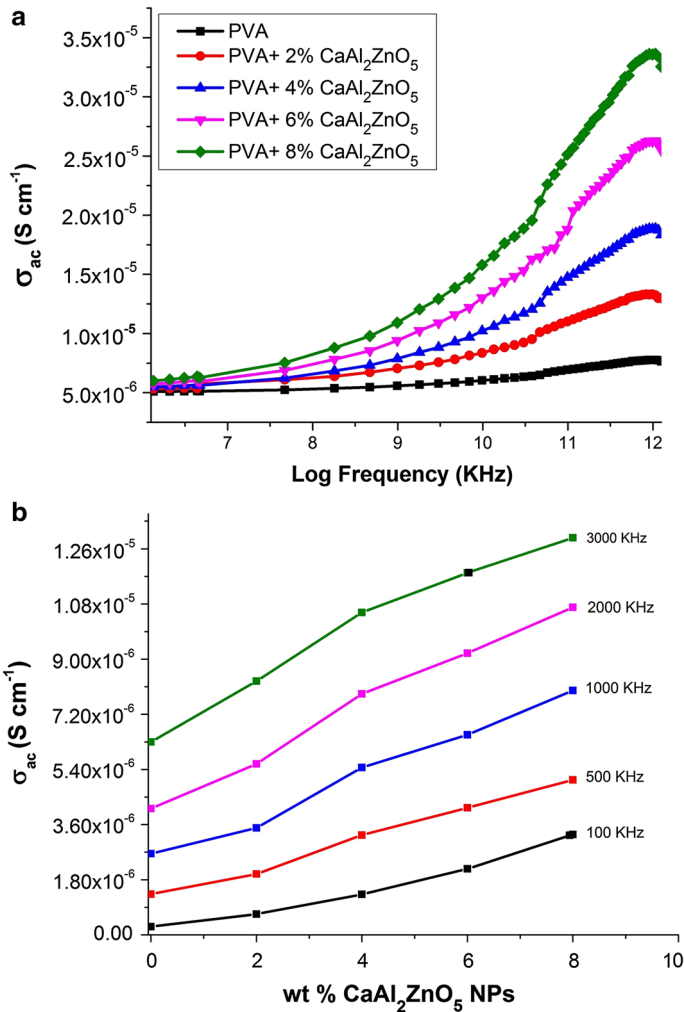
$$\sigma_{ac} = d\,Gs/A \tag{7}$$

Fig. 10 Ac conductivity of PVA/CaAl$_2$ZnO$_5$ NC films as a function of **a** log frequency and **b** different concentration of CaAl$_2$ZnO$_5$ NPs content

where d is film thickness, A is effective cross-sectional area of the sample, and Gs is measured conductance. The improved value of conductivity achieved is 3.35×10^{-5} S cm^{-1} for PVA/8 wt% CaAl$_2$ZnO$_5$ as compared with conductivity of PVA it is 5.3×10^{-6} S cm^{-1} as shown in Fig. 10a. The improved conductivity in this investigation is higher than that reported for PVA/30 wt% TiO$_2$ ($\sigma_{ac} = 2.5 \times 10^{-6}$ S cm^{-1}) reported elsewhere [46].

Figure 11a, b displays an increase in the relative dielectric constant (ε') of PVA/CaAl$_2$ZnO$_5$ NC films with increase in NPs content at lower frequency range which refer to increase in polarization strength, as a result to interaction between dipoles of PVA and nanoparticles. At higher frequency, relative dielectric constant
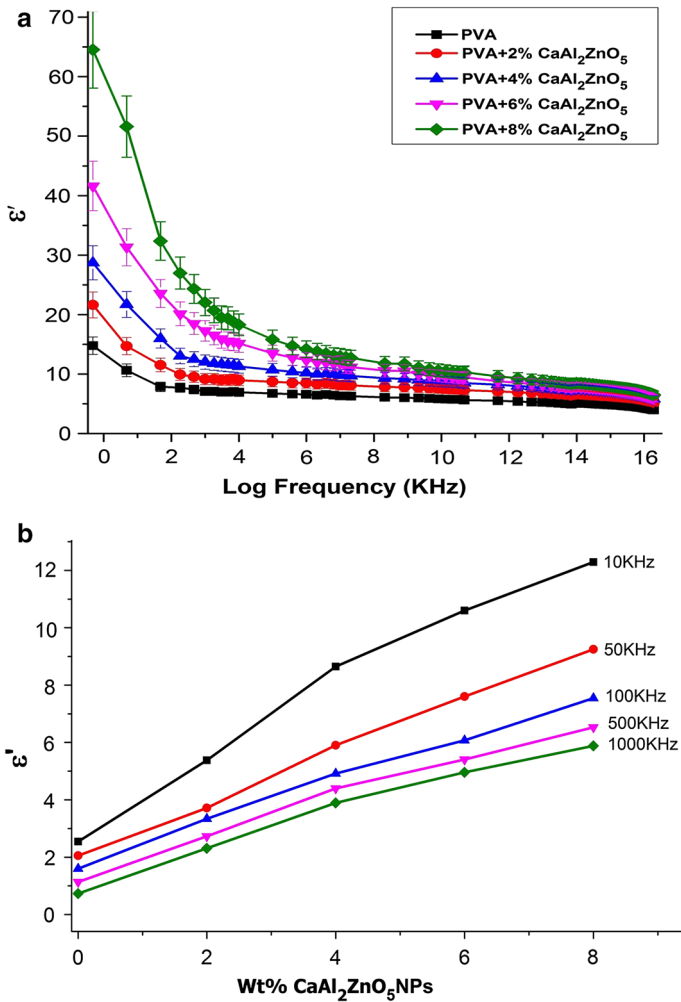
Fig. 11 Relative dielectric constant of PVA/CaAl$_2$ZnO$_5$ NC films as a function of **a** log frequency and **b** different concentration of CaAl$_2$ZnO$_5$ NP contents

(ε') drastically reduced where the dipoles and NPs cannot follow the fast periodic changes in frequency waves. Thus, the NCs exhibit a lower relative dielectric constant (ε') at higher frequencies.

DC (*I–V*) characteristics

The nonlinear current–voltage (*I–V*) behavior provides the theoretical and experimental foundations for the applications of polymer NCs, such as self-regulating heaters, over-current and over-temperature protection devices [47, 48]. Figure 12a shows the *I–V* characteristics for pure PVA and doped with 2, 4, 6 and 8 wt% of
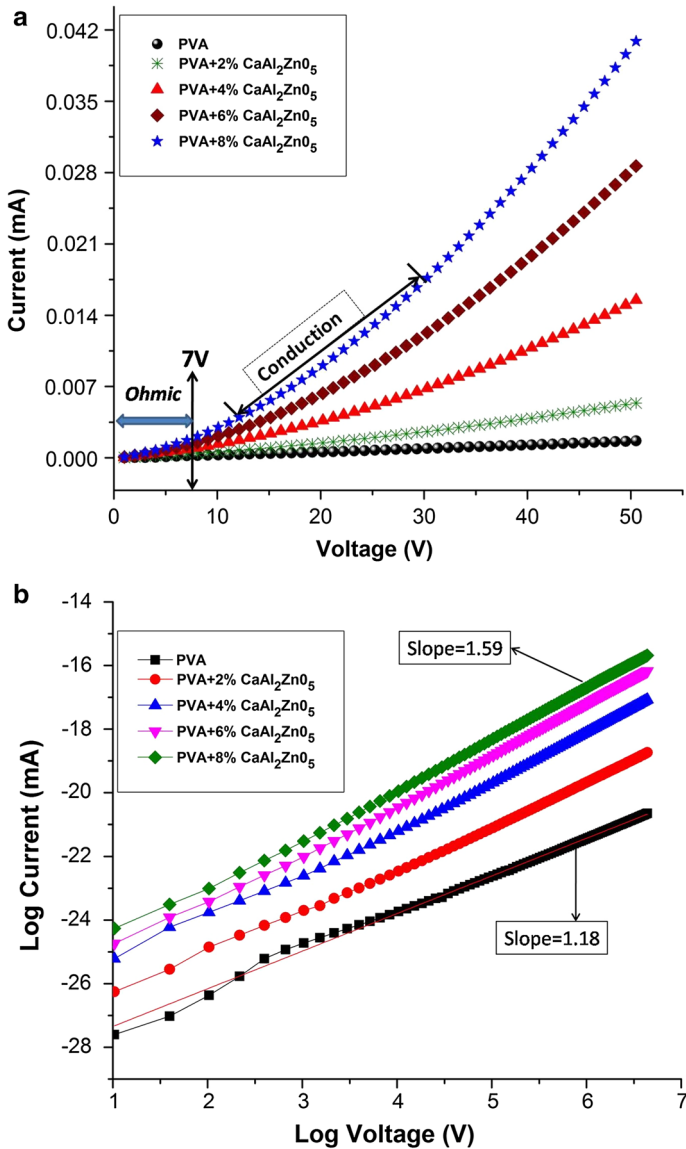
Fig. 12 **a** *I–V* characteristics and **b** logarithmic (*I–V*) for pristine PVA and its nanocomposites at room temperature

$CaAl_2ZnO_5$ NPs at room temperature. It can be noticed from Fig. 12a that there is a continuous increase in conductivity with increase in the dosage of NPs in PVA matrix. When conducting NPs are added in an insulating matrix, the fillers ($CaAl_2ZnO_5$) in the host matrix provide the continuous conductive pathway for the transfer of charge from one particle to another and as a result increase in the conductivity of NC films [49]. In addition, the graph reveals that with increase in the

applied voltage (V) (< 7 V), the current (I) increases gradually, which is expected to refer as Ohmic behavior of NC films. When the applied voltage is > 7 V, a significant increase in current was noticed, which is referred to as conduction behavior. In order to determine the exact mechanism responsible for variation of current with voltage, the typical log (I) versus log (V) curves are plotted (Fig. 12b). It was observed that slope of log (I) versus log (V) curves increases with increase in NPs content in PVA, indicating the reduction in impedance [49, 50]. The log current versus log voltage showed linear behavior, where the slope for doped PVA lies in the range 1.18–1.59, which means the Poole–Frenkel effect is the dominant mechanism for PVA/CaAl$_2$ZnO$_5$ NCs.

Conclusion

The PVA/CaAl$_2$ZnO$_5$ NCs with varying amounts of NPs were prepared by solvent intercalation technique. The effect of different amounts of CaAl$_2$ZnO$_5$ NPs on the structural, opto-electrical and electrochemical properties of the NCs has been studied. The relative dielectric constant of PVA/CaAl$_2$ZnO$_5$ NCs increases with the NPs contents, while it decreases with an increase in applied frequencies; however, ac conductivity of the NCs increases with increase in the NPs dosage and frequency. The FTIR analysis showed a positive interaction between PVA matrix and CaAl$_2$ZnO$_5$ NPs. The energy requirements for optical transitions were found to decrease with an increase in NPs content exhibiting a minimum of 2.8 eV for PVA/8 wt% CaAl$_2$ZnO$_5$ film. The increase in NPs contents brought an increase in RI and reducing band gap energy (E_g). The cyclic voltammetry data exhibited a significant improvement in specific capacitance of PVA/8 wt% CaAl$_2$ZnO$_5$ as compared with pure PVA matrix, which reveals that the investigated NCs are promising materials for energy storage and electrical applications.

References

1. Sadeghi M, Hosseini MH, Tafi H (2013) Synthesis and characterization of ZnCaO$_2$ nanocomposite catalyst and the evaluation of its adsorption/destruction reactions with 2-CEES and DMMP. Int J Bio-Inorg Hybrid Nanomater 2:281–293
2. Liu Y, Zhang H, Zhang Z, Xie Y, Xie E (2010) Conversion of p-type to n-type conductivity in undoped ZnO films by increasing operating temperature. Appl Surf Sci 257:1236–1238
3. Kaidashev EM, Lorenz MV, Von Wenckstern H, Rahm A, Semmelhack HC, Han KH, Grundmann M (2003) High electron mobility of epitaxial ZnO thin films on c-plane sapphire grown by multistep pulsed-laser deposition. Appl Phys Lett 82:3901–3903
4. Zeng YJ, Ye ZZ, Lu JG, Xu WZ, Zhu LP, Zhao BH, Limpijumnong S (2006) Identification of acceptor states in Li-doped p-type ZnO thin films. Appl Phys Lett 89:042106(1–3)
5. Aziz A, Asib NAM, Afaah AN, Mohamed R, Rusop M, Khusaimi Z (2014) Structural and optical properties of ZnO/PMMA nanocomposite. Adv Mater Res 832:602–606
6. Herodotou S, Treharne R, Durose K, Tatlock G, Potter R (2015) The effects of Zr doping on the optical, electrical and microstructural properties of thin ZnO films deposited by atomic layer deposition. Materials 8:7230–7240
7. Kazeminezhad I, Saadatman S, Yousefi R (2016) Effect of transition metal elements on the structural and optical properties of ZnO nanoparticles. Bull Mater Sci 39:719–724

8. Rajeh S, Mhamdi A, Khirouni K, Amlouk M, Guermazi S (2015) Experiments on ZnO: Ni thin films with under 1% nickel content. Opt Laser Technol 69:113–121

9. Lojkowski W, Gedanken A, Grzanka E, Opalinska A, Strachowski T, Pielaszek R, Kurzydłowski KJ (2009) Solvothermal synthesis of nanocrystalline zinc oxide doped with Mn^{2+}, Ni^{2+}, Co^{2+} and Cr^{3+} ions. J Nanopart Res 11:1991

10. Sayari A, Hamoudi S (2001) Periodic mesoporous silica-based organic−inorganic nanocomposite materials. Chem Mater 13:3151–3168

11. Mani GK, Rayappan JBB (2014) Selective detection of ammonia using spray pyrolysis deposited pure and nickel doped ZnO thin films. Appl Surf Sci 311:405–412

12. Pal B, Sarkar D, Giri PK (2015) Structural, optical, and magnetic properties of Ni doped ZnO nano-particles: correlation of magnetic moment with defect density. Appl Surf Sci 356:804–811

13. Tu Y, Zhou L, Jin YZ, Gao C, Ye ZZ, Yang YF, Wang QL (2010) Transparent and flexible thin films of ZnO-polystyrene nanocomposite for UV-shielding applications. J Mater Chem 20:1594–1599

14. Subramani NK, Kasargod Nagaraj S, Shivanna S, Siddaramaiah (2016) Highly flexible and visibly transparent poly (vinyl alcohol)/calcium zincate nanocomposite films for UVA shielding applications as assessed by novel ultraviolet photon induced fluorescence quenching. Macromolecules 49:2791–2801

15. Kim H, Gilmore CM, Horwitz JS, Pique A, Murata H, Kushto GP, Chrisey DB (2000) Transparent conducting aluminum-doped zinc oxide thin films for organic light-emitting devices. Appl Phys Lett 76:259–261

16. Wu C, Cai J, Zhang Q, Zhou X, Zhu Y, Shen PK, Zhang K (2015) Hierarchical mesoporous zinc–nickel–cobalt ternary oxide nanowire arrays on nickel foam as high-performance electrodes for supercapacitors. ACS Appl Mater Interfaces 7:26512–26521

17. Zuo C, Wen J, Zhu S, Zhong C (2010) The effect of C–Al (Ga) co-doping on p-type tendency in zinc oxide by first-principles. Opt Mater 32:595–598

18. Sanchez C, Julian B, Belleville P, Popall M (2005) Applications of hybrid organic–inorganic nano-composites. J Mater Chem 15:3559–3592

19. Kickelbick G (2008) The search of a homogeneously dispersed material—the art of handling the organic polymer/metal oxide interface. J Sol Gel Sci Technol 46:281–290

20. Rudko GY, Kovalchuk AO, Fediv VI, Beyer J, Chen WM, Buyanova IA (2012) Effects of ultravio-let light on optical properties of colloidal CdS nanoparticles embedded in polyvinyl alcohol (PVA) matrix. Adv Sci Eng Med 4:394–400

21. Azizian-Kalandaragh Y, Khodayari A (2010) Ultrasound-assisted preparation of CdSe nanocrystals in the presence of polyvinyl alcohol as a capping agent. Mater Sci Semicond Process 13:225–230

22. Bouropoulos N, Psarras GC, Moustakas N, Chrissanthopoulos A, Baskoutas S (2008) Optical and dielectric properties of ZnO-PVA nanocomposites. Phys Status Solidi A 205:2033–2037

23. Gayitri HM, Al-Gunaid Murad QA, Siddaramaiah B, Gananprakash AP (2019) Structural, dielectric permittivity and optical characteristics of casting poly vinyl alcohol/calcium nickel aluminate nano-composite films. Polym Plast Technol Mater 58:1110–1124

24. Li F, Jiang X, Zhao J, Zhang S (2015) Graphene oxide: a promising nanomaterial for energy and environmental applications. Nano Energy 16:488–515

25. Latif I, AL-Abodi EE, Badri DH, Al Khafagi J (2012) Preparation, characterization and electrical study of (carboxymethylated polyvinyl alcohol/ZnO) nanocomposites. Am J Polym Sci 2:135–140

26. Habibi S, Nematollahzadeh A (2016) Enhanced water flux through ultrafiltration polysulfone mem-brane via addition-removal of silica nano-particles: synthesis and characterization. J Appl Polym Sci 133:43556(1–9)

27. Abdullah OG, Aziz SB, Rasheed MA (2016) Structural and optical characterization of PVA: $KMnO_4$ based solid polymer electrolyte. Results Phys 6:1103–1108

28. Al-Gunaid MQ, Saeed AM, Subramani NK, Madhukar BS (2017) Optical parameters, electrical permittivity and I–V characteristics of PVA/Cs_2CuO_2 nanocomposite films for opto-electronic applications. J Mater Sci: Mater Electron 28:8074–8086

29. Freeda M, Subash TD (2017) Optical characterization of dysporsium doped calcium aluminate nan-ophosphor ($CaAl_2O_4$:Dy) by sol–gel method. Mater Today Proc 4:4290–4301

30. Roy AS, Gupta S, Sindhu S, Parveen A, Ramamurthy PC (2013) Dielectric properties of novel PVA/ZnO hybrid nanocomposite films. Compos Part B Eng 47:314–319

31. Sudhamani SR, Prasad MS, Sankar KU (2003) DSC and FTIR studies on gellan and polyvinyl alco-hol (PVA) blend films. Food Hydrocoll 17:245–250

32. Mansour AF, Mansour SF, Abdo MA (2015) Improvement structural and optical properties of ZnO/PVA nanocomposites. IOSR J Appl Phys 7:60–69

33. Fernandes DM, Hechenleitner AW, Lima SM, Andrade LHC, Caires ARL, Pineda EG (2011) Preparation, characterization, and photoluminescence study of PVA/ZnO nanocomposite films. Mater Chem Phys 128:371–376

34. El Ghoul J (2016) Synthesis, structural and optical properties of nanoparticles (Al, V) co-doped zinc oxide. Bull Mater Sci 39:7–12

35. Samzadeh-Kermani A, Mirzaee M, Ghaffari-Moghaddam M (2016) Polyvinyl alcohol/polyaniline/ZnO nanocomposite: synthesis, characterization and bactericidal property. Adv Biol Chem 6:1–11

36. Chandrakala HN, Ramaraj B (2014) Optical properties and structural characteristics of zinc oxide-cerium oxide doped polyvinyl alcohol films. J Alloys Compd 586:333–342

37. Bello A, Barzegar F, Momodu D, Dangbegnon J, Taghizadeh F, Fabiane M, Manyala N (2015) Asymmetric supercapacitor based on nanostructured graphene foam/polyvinyl alcohol/formaldehyde and activated carbon electrodes. J Power Sources 273:305–311

38. Sathish S, Shekar BC, Kannan SC, Sengodan R, Dinesh KPB, Ranjithkumar R (2015) Wide band gap transparent polymer-inorganic composite thin films by dip-coating method: preparation and characterizations. Int J Polym Anal Charact 20:29–41

39. Chithra MJ, Pushpanathan K, Loganathan M (2014) Structural and optical properties of Co-doped ZnO nanoparticles synthesized by precipitation method. Mater Manuf Process 29:771–779

40. Higashihara T, Ueda M (2015) Recent progress in high refractive index polymers. Macromolecules 48:1915–1929

41. Torres J, Cisneros JI, Gordillo G, Alvarez F (1996) A simple method to determine the optical constants and thicknesses of $Zn_xCd_{1-x}S$ thin films. Thin Solid Films 289:238–241

42. Srivastava S, Haridas M, Basu JK (2008) Optical properties of polymer nanocomposites. Bull Mater Sci 31:213–217

43. Al-Ofi HH, EL-Raheem, Al-Baradi AM, Atta AA (2012) Structural and optical properties of Al_2ZnO_4 thin films deposited by DC sputtering technique. J Non-oxide Glass 3:39–54

44. Masikhwa TM, Madito MJ, Bello A, Dangbegnon JK, Manyala N (2017) High performance asymmetric supercapacitor based on molybdenum disulphide/graphene foam and activated carbon from expanded graphite. J Colloid Interface Sci 488:155–165

45. Ravikiran YT, Lagare MT, Sairam M, Mallikarjuna NN, Sreedhar B, Manohar S, Aminabhavi TM (2006) Synthesis, characterization and low frequency AC conduction of polyaniline/niobium pentoxide composites. Synth Met 156:1139–1147

46. Mahendia S, Tomar A, Kumar S (2010) Electrical conductivity and dielectric spectroscopic studies of PVA–Ag nanocomposite films. J Alloys Compd 508:406–411

47. Anandraj J, Joshi GM (2017) Zirconia sulphate dispersed polymer composites for electronic applications. J Inorg Organomet Polym Mater 27:1835–1850

48. Al-Gunaid MQ, Saeed AM (2018) Effects of the electrolyte content on the electrical permittivity, thermal stability, and optical dispersion of poly (vinyl alcohol)–cesium copper oxide–lithium perchlorate nanocomposite solid-polymer electrolytes. J Appl Polym Sci 13:45852(1–14)

49. Zhang J, Feng D, Feng S, Han J, Diao G, Liu D (2008) Correlation between current–voltage (I–V) characteristic in the electric–thermal equilibrium state and resistivity-temperature behavior of electro-conductive silicone rubber. J Appl Polym Sci 107:2053–2057

50. Saini I, Sharma A, Rozra J, Dhiman R, Aggarwal S, Sharma PK (2015) Modification of structural, thermal, and electrical properties of PVA by addition of silicon carbide nanocrystals. J Appl Polym Sci 132:42464(1–8)

Affiliations

H. M. Gayitri[2] · Murad AL-Gunaid[3,4] · Siddaramaiah[4] · A. P. Gnana Prakash[1]

[1]   Department of Studies in Physics, University of Mysore, Manasagangotri, Mysore 570006, India

[2]   Department of Electronics and Communication Engineering, Sri Jayachamarajendra College of Engineering, JSS Science and Technology University, Mysore 570006, India

[3]   Department of Chemistry, Faculty of Education, Thamar University, Dhamar, Yemen

[4]   Department of Polymer Science and Technology, Sri Jayachamarajendra College of Engineering, JSS Science and Technology University, Mysore 570006, India